Communication

Bioconversion of Glycerol to 1,3-Propanediol Using *Klebsiella pneumoniae* L17 with the Microbially Influenced Corrosion of Zero-Valent Iron

Da Seul Kong [1], Minsoo Kim [1], Shuewi Li [1], Sakuntala Mutyala [1] (ID), Min Jang [2], Changman Kim [3,4,*] (ID) and Jung Rae Kim [1,*] (ID)

[1] School of Chemical Engineering, Pusan National University, Busan 46241, Republic of Korea
[2] Department of Environmental Engineering, Kwangwoon University, 20 Kwangwoon-Ro, Nowon-Gu, Seoul 01897, Republic of Korea
[3] Advanced Biofuel and Bioproducts Process Development Unit, Lawrence Berkeley National Laboratory, Emeryville, CA 94608, USA
[4] Department of Biotechnology and Bioengineering, Chonnam National University, Gwangju 61188, Republic of Korea
* Correspondence: cmkim@jnu.ac.kr (C.K.); j.kim@pusan.ac.kr (J.R.K.); Tel.: +1-510-332-0104 (C.K.); +82-51-510-2393 (J.R.K.); Fax: +82-51-512-8563 (C.K. & J.R.K.)

Abstract: The bacterial redox state is essential for controlling the titer and yield of the final metabolites in most bioconversion processes. Glycerol conversion to 1,3-propanediol (PDO) requires a large amount of reducing equivalent and the expression of reductive pathways. Zero-valent iron (ZVI) was used in the glycerol bioconversion of *Klebsiella pneumoniae* L17. The level of 1,3-PDO production increased with the oxidation of ZVI (31.8 ± 1.2 vs. 25.7 ± 0.5, ZVI vs. no ZVI) while the cellular $NADH/NAD^+$ level increased (0.6 vs. 0.3, ZVI vs. no ZVI). X-ray diffraction showed that the iron oxide (Fe_2O_3) was formed during glycerol fermentation. L17 obtained electrons from ZVI and dissolved the iron continuously to form cracks on the surface, suggesting microbially influenced corrosion (MIC) was involved on the surface of ZVI. The ZVI-implemented fermentation shifted bioconversion to a more glycerol-reductive pathway. The qPCR-presented glycerol dehydratase (DhaB) with ZVI implementation was strongly expressed compared to the control. These results suggest that ZVI can contribute to the biotransformation of PDO by inducing intracellular metabolic shifts. This study could also suggest a novel microbial fermentation strategy with the application of MIC.

Keywords: metabolic shift; zero-valent iron (ZVI); iron-supported bioconversion; *Klebsiella pneumoniae* L17' 1,3-propanediol(1,3-PDO); glycerol

1. Introduction

The cost of steel destruction and replacement induced by corrosion accounts for approximately 3% of global gross domestic product [1,2]. Microbe–metal interactions are an essential ecological niche in the earth's biogeochemical cycles for metal and metalloid compounds. The worldwide cost of microbially influenced corrosion (MIC) is reaching billions of dollars per year [3,4]. Various microorganisms involved in MIC have been reported to be iron-oxidizing (IOB), sulfate-reducing (SRB), nitrate-reducing (NRB), acid-producing (APB), and metal-oxidizing bacteria (MOB), as well as methanogens, fungi, and even archaea [5–8]. MIC can transfer respiratory electrons anaerobically from the metallic iron surface to a cell, where energetically favorable redox reactions proceed and provide respirational energy for the cellular metabolism, called electrical MIC (EMIC) [3,9–12]. IOB oxidizes iron species using organic matter (e.g., glycerol) to synthesize biomass [13]. IOBs frequently form a gelatinous or fibrous outer layer that provides a favorable anaerobic environment such as a micro-electrochemical cell [14]. Electrons from iron oxidation are

delivered to iron oxidase or c-type cytochromes on the outer membrane and reduce NAD^+ to NADH by inner membrane NADH dehydrogenase [15–17]. Other reports showed that such iron oxidation shifts the bacterial metabolic pathway and influences the intracellular redox state [18–21].

1,3-Propanediol (1,3-PDO; $C_3H_8O_2$) is an important intermediate in the synthesis of polymers and value-added chemicals needed to replace petrochemical-based platform compounds [22,23]. 1,3-PDO is used widely in the industrial production of polyester polytrimethylene terephthalate (PTT) [24,25]. The biosynthesis of 1,3-PDO uses the glycerol-reductive pathway via 3-HPA (Equations (1) and (2)) [26,27]. The continuous reproduction of NADH is essential for the efficient production of PDO [28–30]. Various strategies for regenerating NADH from NAD^+ for PDO production have been reported [19,30]. *K. pneumoniae* is used as a biocatalyst for glycerol conversion to synthesize glycerol derivatives, such as 1,3-PDO and 3-HP, owing to its highly developed anaerobic glycerol assimilation capability. Among *K. pneumoniae* strains, *K. pneumoniae* L17 can transfer their residual electron to extracellular metallic compounds (or carbon electrode) [24,28,31,32]. Electro-fermentation could control the bacterial redox balance to increase the productivity of value-added chemicals in bioconversion [18,32–35]. On the other hand, MIC-driven bioconversion and fermentation have not been studied extensively. The concept of MIC can be applied easily to bioconversion by adding powder or granule-type metal compounds to a bioreactor.

$$\text{Glycerol}(C_3H_8O_3) \rightarrow \text{3-HPA } (C_3H_6O_2) + H_2O \tag{1}$$

$$\text{3-HPA}(C_3H_6O_2) + 2NADH \rightarrow \text{1,3-PDO}(C_3H_8O_2) + 2NAD^+ \tag{2}$$
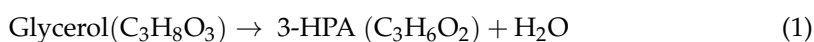
This study evaluated the bioconversion of glycerol to PDO using zero-valent iron (ZVI) as a reducing reagent. Previous studies optimized fermentation with ZVI in minimal media without a vitamin and trace elemental solution under various conditions (e.g., oxygen and pH) [28,36]. The present study examined the mechanism of the cellular metabolism and iron ion dynamics (Fe^{2+} and Fe^{3+} from ZVI oxidation) during MIC. The bacterial metabolic shift induced by ZVI was first evaluated. The transcription level and metabolite-based mathematic model were investigated in *Klebsiella pneumoniae* L17. The changes in dissolved ferric (Fe^{3+}) and ferrous (Fe^{2+}) ions and ZVI surface analysis indicated the dynamics of iron species in glycerol conversion. These results contribute to the development of a novel microbial conversion and fermentation by applying MIC.

2. Materials and Method

2.1. Strain and Cultivation

The source of *K. pneumoniae* L17 was the China Center for Type Culture Collection (CCTCC). Luria Bertani (LB) medium was used for the preculture and seed culture of *K. pneumoniae* L17. The fermentation medium for flask experiments has a composition of 18.04 g K_2HPO_4, 1.804 g KH_2PO_4, 1 g NaCl, 1 g NH_4Cl, 0.2 g yeast extract, 0.25 g $MgSO_4 \cdot 7H_2O$, 9.2 g pure glycerol, 1.25 mL 100× vitamin solution (per liter: biotin 2 mg, folic acid 2 mg, pyridoxine hydrochloride 10 mg, thiamine hydrochloride 5 mg, nicotinic acid 5 mg, D, L-calcium pantothenate 5 mg, vitamin B_{12} 0.1 mg, p-aminobenzoic acid 5 mg, and lipoic acid 5 mg) and 1.25 mL 100× trace element solution (per liter: nitrilotriacetic acid 1 g, $MgSO_4 \cdot 7H_2O$ 3 g, $MnSO_4 \cdot 2H_2O$ 0.5 g, NaCl 1 g, $FeSO_4 \cdot 7H_2O$ 0.1 g, $CoSO_4$ 0.1 g, $CaCl_2$ 0.1 g, $CuSO_4 \cdot 5H_2O$ 0.01 g, $Al \cdot K(SO_4)_2$ 0.01 g, H_3BO_3 0.01 g, $NiCl_2$ 0.024 g, Na_2WO_4 0.025 g, $ZnCl_2$ 0.13 g, and $Na_2MoO_4 \cdot 2H_2O$ 0.025 g). HCl (10%) and NaOH (5 N) solutions were used to adjust the pH of the medium to 7.5. ZVI (0.5 g, 70 mesh powder, <212 micrometer, ACROS, New Jersey, NJ, USA), ferric chloride (0.2 g, $FeCl_3$, Duksan, Ansansi, gyunggido, Korea), and ferrous chloride tetrahydrate (0.31 g, $FeCl_2 \cdot 4H_2O$, Fisher Chemical, Waltham, MA, USA) were added as an external iron supplement as an electron donor. *K. pneumoniae* L17 (hereinafter L17) was cultured in a shaking incubator at 200 rpm and 30 °C. Anaerobic cultivation was carried out after nitrogen purging into the headspace of a cultivation serum bottle (200 mL) for 10 min. The initial cell density of the culture was adjusted to 0.05 OD_{600}.

2.2. Analytical Methods

The liquid samples were taken at 0, 5, 10, and 24 h to determine the cell density and metabolite production. The cell density (OD_{600}) was measured using a UV-Vis spectrophotometer (Optizen POP, Keen Innovative Solutions, Daejeon, Korea). Metabolite production was identified by centrifuging each liquid sample at 5000 rpm for 10 min, diluting the supernatants, and filtering them through a syringe filter. The samples were analyzed by high-performance liquid chromatography (HPLC, HP 1160 series, Agilent Technologies, Santa Clara, CA, USA) equipped with a 300 × 7.8 mm Aminex HPX-87H (Bio-Rad, Hercules, CA, USA) column at 65 °C and a refractive index (RI) and photodiode array (PDA) detector, using 2.5 mM H_2SO_4 as the mobile phase (flow rate = 0.5 mL/min). The concentrations of total dissolved iron and ferrous ions (Fe^{2+}) were quantified using colorimetric methods [28]. The iron species in solution were measured using a Fe ion kit (HS-Fe(T), HUMAS, Daejeon, Korea) and Fe^{2+} ions kit (HS-Fe (2+), HUMAS, Daejeon, Korea). Fe^{3+} was calculated by subtracting the measured Fe^{2+} from the total iron concentration. Powder X-ray diffraction (XRD, X'Pert-MPD, PHILIPS, Amsterdam, Netherlands) was performed using Cu-Kα (λ = 0.15406 nm) operated at 40 kV and 30 mA. Metabolic flux analysis (MFA) was investigated, as described elsewhere [37]. All the equations for the undetermined metabolic pathway were solved by linear optimization using the MetaFluxNet program [38]. $NADH/NAD^+$ ratio was measured using a colorimetric kit (K337-100, Biovision, Milpitas, CA, USA) [18].

2.3. Real-Time qPCR

The cells were harvested from late-exponential growth phases to analyze the expression level of each gene in the glycerol fermentation pathway. The culture was centrifuged at 8000 rpm for two minutes. The harvested pellet was processed for RNA isolation using a total isolation kit (TransZol UP, TRAN, Beijing, China). RNA was measured and calculated by nano-drop (NanoDrop One^c, Thermo Scientific, Waltham, MA, USA) for the same sample concentration. The estimated amount of RNA was synthesized into cDNA using the first-strand cDNA synthesis system (iSccript cDNA synthesis kit, BIO-RAD, Hercules, CA, USA). qPCR analysis was performed using the SYBR green method in the StepOnePlus Real-Time PCR system (Applied Biosystems, Waltham, MA, USA). Each 20 μL sample of reaction mixture contained 300 ng of cDNA, 10 μL of 2xPower SYBR Green PCR Master Mix (Applied Biosystems, Waltham, MA, USA), 5 pmol of forward and reverse primers, and DEPC-treated water. The thermal cycling conditions were as follows: one cycle of denaturation at 95 °C for 30 s; 40 cycles of amplification at 95 °C for 15 s, 62 °C for 30 s, and 72 °C for 30 s. The relative quantification of the mRNA levels was calculated using the $\Delta\Delta C_t$ method [36]. All analyses were carried out in duplicate.

3. Results and Discussion

3.1. Metabolic Profile of K. pneumoniae L17 with ZVI

Three different iron species (ZVI (Fe^0), Fe^{2+}, and Fe^{3+}) were added for anaerobic glycerol fermentation. Most of the glycerol was consumed in all bottles (104.3 ± 1.2, 102.3 ± 0.2, and 102.8 ± 0.1 for glycerol consumption in the control, ZVI, ferrous and ferric, respectively) within 24 h. Consequently, PDOs were produced to 25.7 ± 0.5, 31.8 ± 1.2, 27.5 ± 0.4, and 25.8 ± 0.1 mM in the control, ZVI, ferrous (Fe^{2+}), and ferric (Fe^{3+}), respectively. The yield of PDO production was 1.3 times higher with ZVI (0.31 PDO production mole/glycerol consumption mole) than with the control (0.24). Figure 1 and Table S1 present the metabolite productions. Interestingly, the metabolic profiles of L17 with more oxidized iron species (Fe^{2+} and Fe^{3+}) showed similar glycerol consumption and PDO production to the control. This indicates that L17 can uptake electrons from a solid granule of more reduced iron (ZVI) rather than the oxidized form of dissolved Fe^{2+} and Fe^{3+}. The metabolic flux model was suggested to estimate the fluxes in bioconversion and the microbial redox states of the oxidative and reductive pathways (Figure 2). ZVI shifted the metabolic flux toward more reductive pathways (30.6 and 46.9 in the control and ZVI, respectively). Kim et al.

reported that under cathodic glycerol fermentation, electrode-based electron transfer drives the metabolic shift of L17 from 30:70 (reductive to oxidative pathways) under open circuit conditions (non-BES) to 40:60 under cathodic conditions (BES) [24]. In this study, only 0.23 mmol of electron transfer resulted in 6.1 mmol of PDO increase. Here, ZVI played a similar role to the electrode to provide electrons to the cell continuously while inducing a shift in metabolic flux (Figure 2).
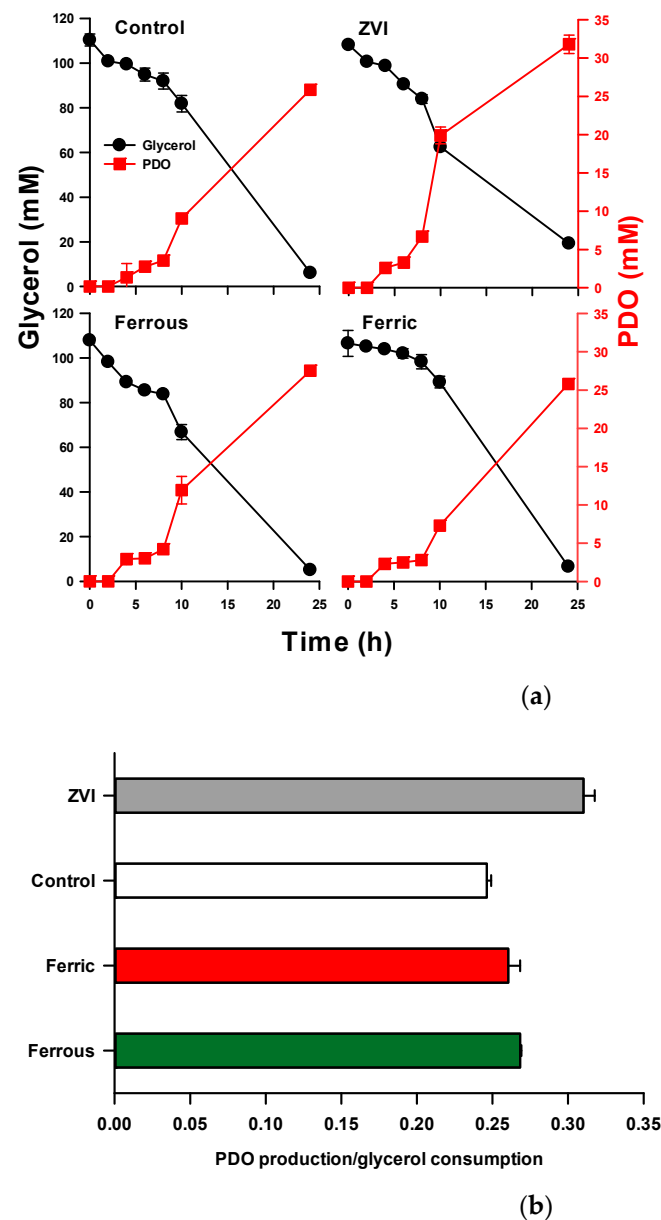

(a)

(b)

Figure 1. Metabolite production of *K. pneumoniae* L17 using iron species (ZVI, ferrous, ferric, without iron). (**a**) Glycerol consumption and PDO production; (**b**) 1,3-PDO production yield with iron species (ZVI, ferrous, ferric, and control). ZVI was used as an electron donor for bacteria, while the control did not contain ZVI. Ferric (Fe^{3+}) in the form of $FeCl_3$ (Fe^{2+}) and ferrous in the form of $FeCl_2 \cdot 4H_2O$ were used as alternative iron species to ZVI (Fe^0).
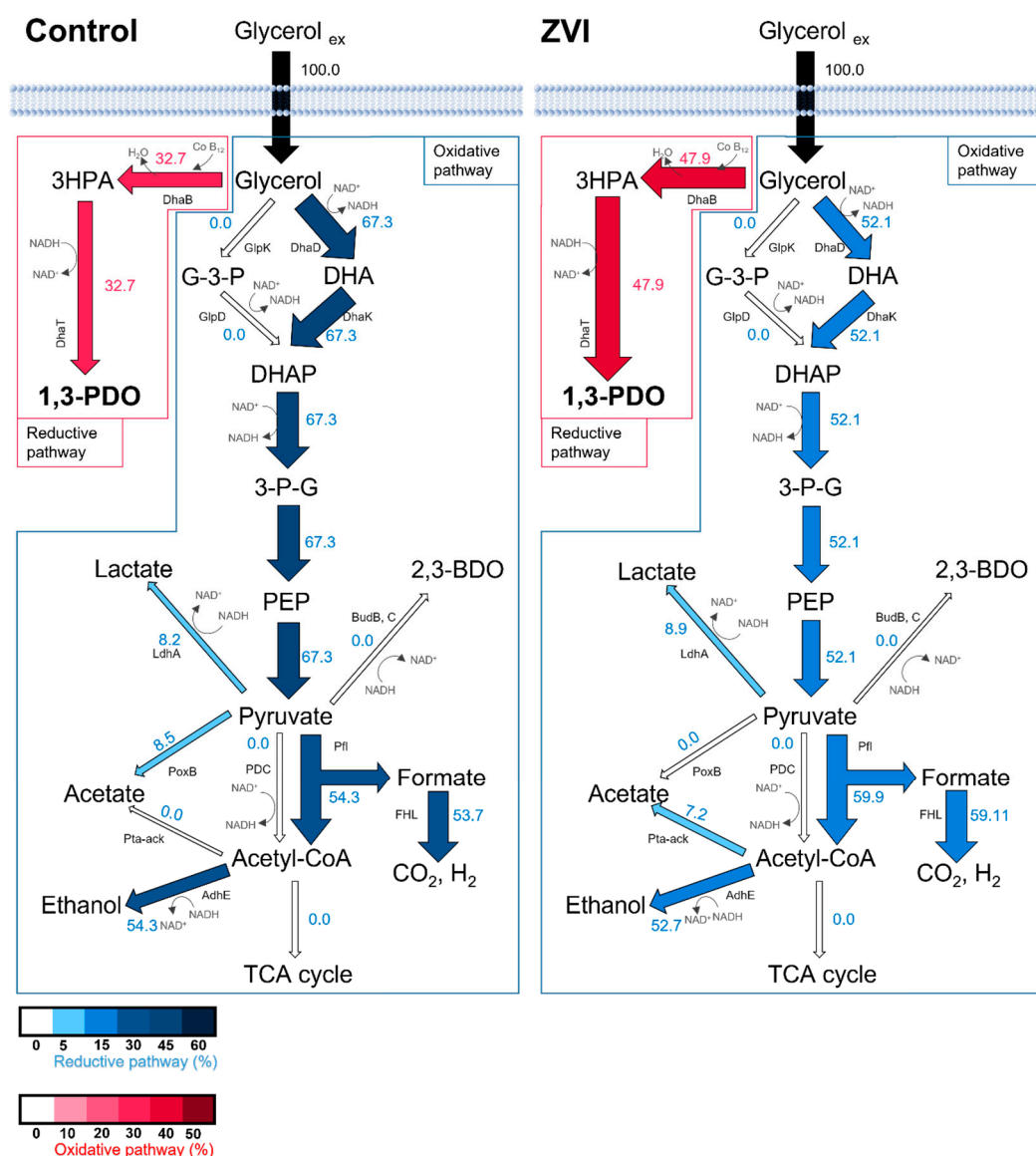
Figure 2. Metabolic flux analysis with and without ZVI, which was calculated using the meta flux net program. (Control) without ZVI and (ZVI) with ZVI in the reactor. Glycerol$_{ex}$ indicates that glycerol existed outside of the cell membrane.

3.2. Change of Bacterial Redox State by ZVI

The bacterial redox state is influenced by external reducing and oxidizing reagents in glycerol bioconversion. A previous study showed that the NADH/NAD$^+$ ratio, representing the cellular redox state, was controlled by the potential applied to the electrode [37]. Similar to previous work, Figure 3 showed that the NADH/NAD$^+$ ratio with ZVI was relatively higher than that in the control. The intracellular electron transfer of L17 under ZVI maintained a high NADH/NAD$^+$ level throughout fermentation. A more reduced environment shifted glycerol conversion toward the reductive pathway. Under anaerobic conditions, L17 converts glycerol to two alcoholic metabolites, PDO and ethanol, by alcohol dehydrogenases with NADH as a cofactor, which is more favorable under high cytoplasmic NADH/NAD$^+$ ratios. The net NADH changes in PDO and ethanol production were -1 and 0, respectively; PDO production is preferred to reduce the cytoplasmic NADH level. When additional reducing energy was added to the cytoplasm by ZVI oxidation, the cytoplasmic NADH/NAD$^+$ ratio would increase, and the metabolic fluxes would shift to maintain the cellular redox homeostasis. PDO production would decrease the

cytoplasmic $NADH/NAD^+$ ratio with the concomitant regeneration of NADH. Although the increase in PDO production in ZVI-implemented fermentation was identified, a high $NADH/NAD^+$ ratio was maintained compared to the control. This result suggests the following: (1) the steady supplement of electrons into L17 or (2) insufficient catalytic activity of the glycerol-reductive pathway to resolve the high $NADH/NAD^+$ ratio.
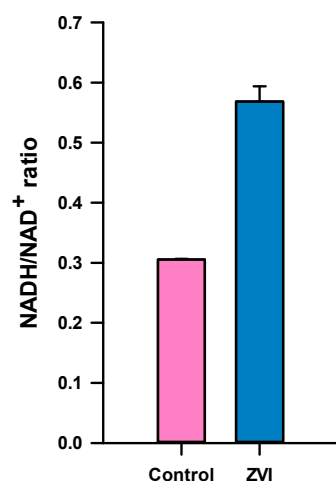

Figure 3. $NADH/NAD^+$ ratio with and without ZVI. (Control) without iron in the reactor and (ZVI) with ZVI in the reactor.

The redox-related metabolic response to maintain redox homeostasis is usually initiated by the transcription level. L17 has three major modules (enzymes) to initiate glycerol conversion depending on the cell conditions: aerobic (via GlpK), anaerobic oxidation (via DhaD), and anaerobic reduction (via DhaB). The transcriptional analysis of such enzymes was carried out to reveal the metabolic response against ZVI implementation. Figure 4 presents the comparative mRNA level of the three enzymes. Interestingly, the expression of glycerol dehydratase (dhaB), the first enzyme of glycerol reduction, was approximately three times higher with ZVI than with the control.
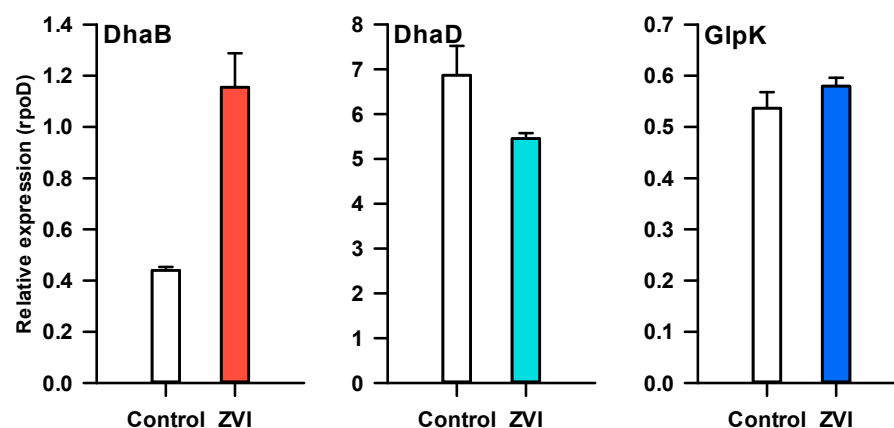

Figure 4. mRNA expression profiles for glycerol-converting enzymes (glpK, dhaD, and dhaB) with ZVI and without ZVI. (Control) without iron in the reactor and (ZVI) with ZVI in the reactor.
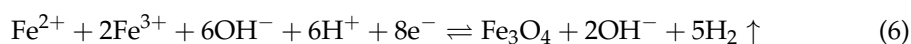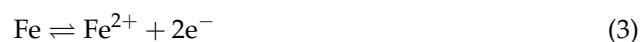
In contrast, glycerol dehydrogenase (dhaD) for anaerobic glycerol oxidation was less expressed with ZVI than the control. This result suggests that ZVI-driven electron transfer shifts the conversion toward the reductive metabolism. Although the glycerol-reductive pathways are well expressed with ZVI, the $NADH/NAD^+$ ratio was still high (Figure 3). Therefore, PDO production was insufficient to release the intracellular redox

stress induced by ZVI. The glycerol consumption and PDO production were similar under higher coenzyme B_{12} levels, an essential cofactor for glycerol bioconversion (Figure S1).

The ZVI and control cultures expressed similar glycerol kinase (glpK) levels. The glpK phosphorylates glycerol to synthesize glycerol-3-phosphate (G-3-P) in the glp module. G-3-P is oxidized further by glycerol-3-phosphate dehydrogenase (glpD) to synthesize dihydroxyacetone-phosphate (DHAP). GlpR (glycerol-3-phosphate regulon repressor) inhibits the expression of glp regulon. GlpR has a high affinity with G-3-P, and the complex formation of G-3-P and GlpR prevents the expression inhibition of the glp module enzymes (glpK and glpD) [39]. The Glp module functions under aerobic and anaerobic respiratory conditions [40]. Therefore, anaerobic and additional reducing supplement conditions, both ZVI and an electrode, did not influence glpK expression significantly.

3.3. Oxidation of ZVI by Microbially Influenced Corrosion (MIC)

Figures 5 and S2 show the change in soluble iron species in the culture medium during the experiment. When ZVI was implemented in L17 (biotic), the level of Fe^{2+} increased over 10 h, whereas it did not increase in the abiotic and inactive cultures (Figure 5). This result indicates that the bacterial activity oxidized ZVI for their metabolism. On the other hand, the dissolved iron in the media decreased regardless of the cell throughout cultivation, probably due to the precipitation of Fe_2O_3 or Fe_3O_4 (Figures 5 and S2). In a separate experiment, when ZVI was autoclaved for sterilization, the pH increased slightly from 7.5 to 8.2. This result can be attributed to the substances inside the culture medium reacting with ZVI at high temperatures; ZVI is oxidized (Equations (3) or (4)), and water is decomposed (Equation (5)) to form iron oxide (Fe_3O_4 or Fe_2O_3). The generated OH^- increases the pH of the culture medium with the accumulation of H_2 in the headspace (Equations (6) or (7)) (Figure S3) [41–43].

$$Fe \rightleftharpoons Fe^{2+} + 2e^- \tag{3}$$

$$Fe \rightleftharpoons Fe^{3+} + 3e^- \tag{4}$$

$$H_2O \rightleftharpoons OH^- + H^+ \tag{5}$$

$$Fe^{2+} + 2Fe^{3+} + 6OH^- + 6H^+ + 8e^- \rightleftharpoons Fe_3O_4 + 2OH^- + 5H_2 \uparrow \tag{6}$$

$$2Fe^{3+} + 5OH^- + 5H^+ + 6e^- \rightleftharpoons Fe_2O_3 + 2OH^- + 4H_2 \uparrow \tag{7}$$

XRD was carried out on the iron oxide precipitates on the bottom of the culture: abiotic ZVI with non-sterilization (ab-ZVI-ns); abiotic ZVI with sterilization (ab-ZVI-s); ZVI after 24 h culture without bacteria (ab-ZVI-24h), and ZVI after 24 h culture with bacteria (bio-ZVI-24h) [44]. The peak intensity for Fe_2O_3 was lower in ab-ZVI-ns, while it was higher in bio-ZVI-24h (Figure 6), but the peak for Fe_3O_4 was negligible (Figure S4). Fe^{2+} was oxidized further to Fe^{3+} and precipitated in the form of Fe_2O_3. With the other form of flat-type ZVI specimen, cracks were found from 10 and 24 h of cultivation with L17 (Figure 7). L17 dissolves iron continuously from the ZVI surface by oxidation and eventually fractures the specimen. This crack formed under the anaerobic environment. The first hypothesis is that L17 attaches to the surface of the ZVI specimen to exchange electrons by oxidation and then detaches from the surface (Figure 8A) [45,46]. The second is that MIC is initiated by bacterial attachment (cathode site), which continuously drives electron flow from the neighboring anode site [9,47,48]. The continuous oxidation of iron by MIC eventually forms a linear crack, as shown in Figure 8B. More cracks formed at bio-ZVI-24h than at 10 h (Figure 7).
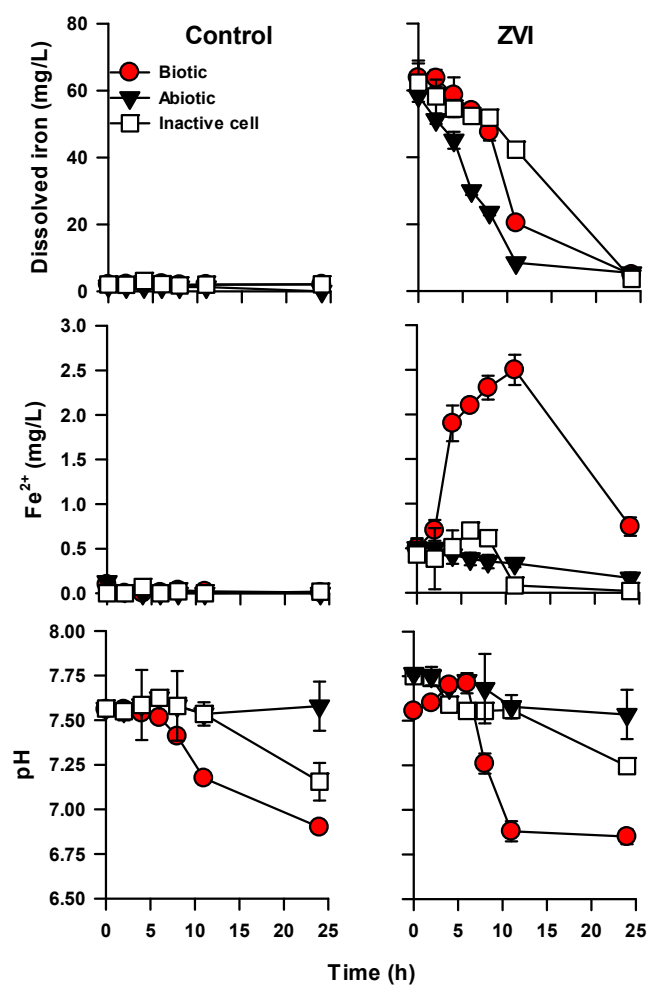
Figure 5. Changes in the iron concentration (dissolved iron and Fe^{2+}) and pH for the control (without iron), and with ZVI during glycerol fermentation.
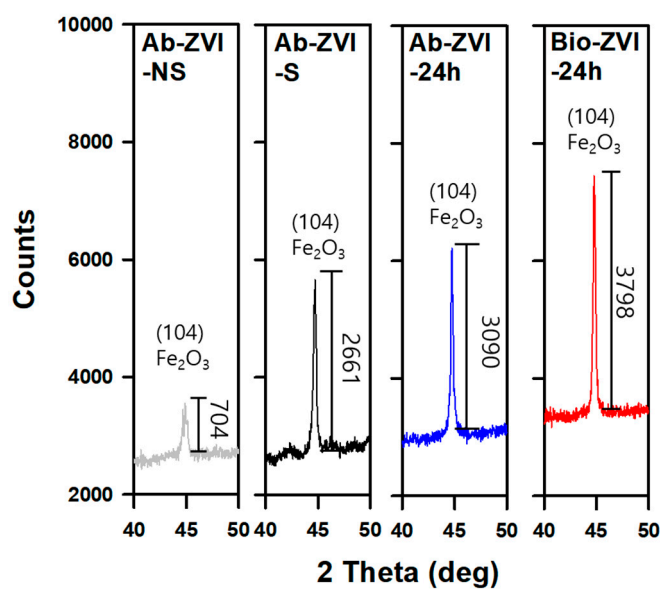

Figure 6. XRD pattern of iron precipitation of ab-ZVI-ns, ab-ZVI-s, ab-ZVI-24h, and bio-ZVI-24h.
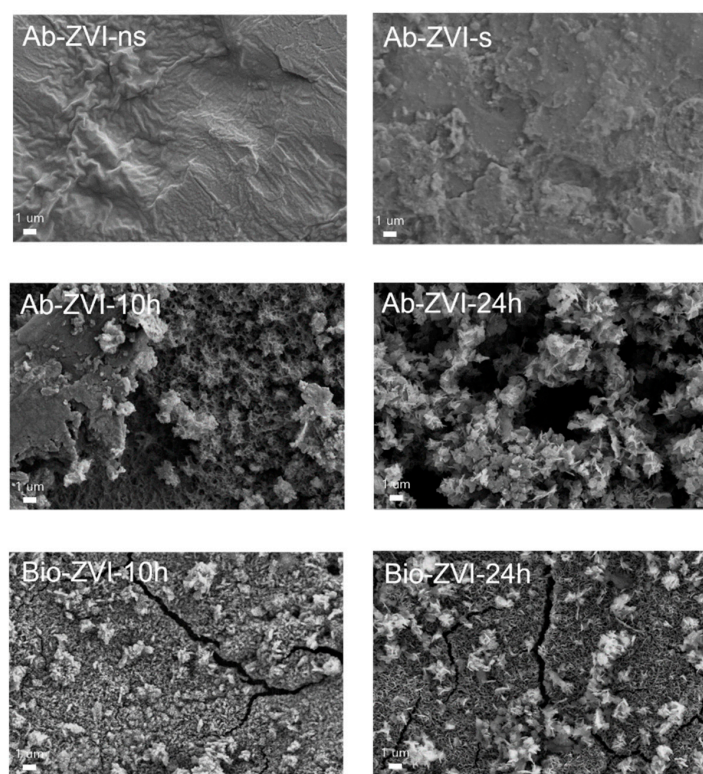
Figure 7. FE-SEM images of the surface of the ZVI specimen before the experiment, ZVI after sterilization, and during the abiotic and biotic culture for 10 h and 24 h.
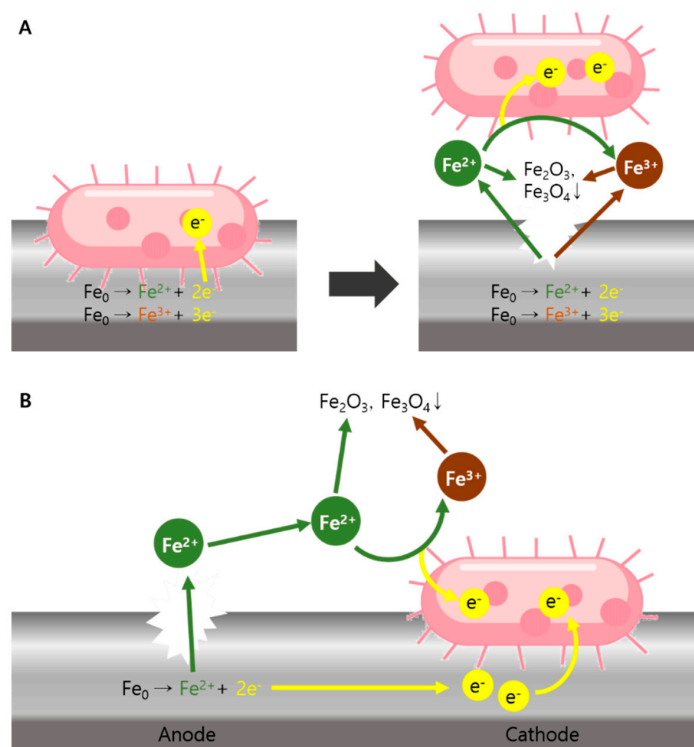

Figure 8. Schematic diagram of microbiologically influenced corrosion (MIC) for L17 at ZVI. (**A**) cell attaches to the surface of the ZVI specimen to exchange electrons by oxidation and then detaches from the surface. (**B**) Microbially influenced corrosion (MIC) is initiated by bacterial attachment (cathode site), which continuously drives electron flow from the neighboring anode site.

Microbially influenced corrosion (MIC) of ZVI provide electrons to activate the glycerol-reductive pathway and simultaneously increase 1,3-PDO production. These results showed that *Klebsiella pneumoniae* L17, which was previously known as a glycerol fermenter, can uptake respiratory electrons from MIC and drive bioconversion to a more reductive pathway. The MIC with bioconversion changes the surface morphology of ZVI. Although L17 was reported to be active in using carbon electrodes as the electron acceptor and donor in a bioelectrochemical system, it could also oxidize iron species under an anaerobic environment in this study. Hence, the corrosion proceeds by a wider range of bacterial species, including fermentative strains over the conventionally known iron-oxidizing bacteria. The ZVI has been studied extensively as a reducing reagent in environmental applications. Thus, it can also be applied to bioconversion and fermentation. Value-added chemicals can be produced by providing cost-effective iron powder, such as ZVI, in fermenters and bioprocesses. The cost of iron powder (ZVI) is approximated at USD 7.6/kg with considering the higher market price of 1,3-PDO (USD 194/kg). Only 0.5 g per flask (approx. 0.38 cent) was implemented for general culture in this study. Although further development of scaled-up fermenter and process should be carried out, this work has shown the feasibility of ZVI application to glycerol conversion.

4. Conclusions

This study examined the cellular metabolism and dynamics of ZVI oxidation during glycerol conversion by *Klebsiella pneumonia* L17. L17 receives reductive energy from ZVI oxidation to increase the NADH level within cells. The $NADH/NAD^+$ ratio changes from 0.3 (control) to 0.6 (with ZVI) when ZVI is provided, and L17 prefers the reductive pathway to consume NADH (32.7%:47.9%, control: with ZVI, metabolic flux). Therefore, the increase in glycerol dehydratase (DhaB) was observed in ZVI compared to the control using qPCR. In particular, L17 oxidizes ZVI and forms cracks on the ZVI surface. XRD revealed Fe_2O_3 to be the solid iron species in the bottle. These results suggest that reductive iron species, such as ZVI, induce an intracellular metabolic shift in bioconversion. These results show that the microbially influenced corrosion (MIC)-driven bioconversion helps control the redox balance in microbial fermentation. This study is also expected to develop a novel microbial fermentation strategy using cost-effective reducing agents, such as ZVI.

References

1. Koch, G. Cost of corrosion. In *Trends in Oil and Gas Corrosion Research and Technologies*; Elsevier: Amsterdam, The Netherlands, 2017; pp. 3–30.
2. Hou, B.; Li, X.; Ma, X.; Du, C.; Zhang, D.; Zheng, M.; Xu, W.; Lu, D.; Ma, F. The cost of corrosion in China. *NPJ Mater. Degrad.* **2017**, *1*, 4. [CrossRef]
3. Emerson, D. The role of iron-oxidizing bacteria in biocorrosion: A review. *Biofouling* **2018**, *34*, 989–1000. [CrossRef] [PubMed]
4. Little, B.; Blackwood, D.; Hinks, J.; Lauro, F.; Marsili, E.; Okamoto, A.; Rice, S.; Wade, S.; Flemming, H.-C. Microbially influenced corrosion—Any progress? *Corros. Sci.* **2020**, *170*, 108641. [CrossRef]
5. Mand, J.; Park, H.S.; Jack, T.R.; Voordouw, G. The role of acetogens in microbially influenced corrosion of steel. *Front. Microbiol.* **2014**, *5*, 268. [CrossRef]
6. Xu, D.; Li, Y.; Song, F.; Gu, T. Laboratory investigation of microbiologically influenced corrosion of C1018 carbon steel by nitrate reducing bacterium Bacillus licheniformis. *Corros. Sci.* **2013**, *77*, 385–390. [CrossRef]
7. Liu, B.; Li, Z.; Yang, X.; Du, C.; Li, X. Microbiologically influenced corrosion of X80 pipeline steel by nitrate reducing bacteria in artificial Beijing soil. *Bioelectrochemistry* **2020**, *135*, 107551. [CrossRef]
8. Qian, H.; Zhang, D.; Lou, Y.; Li, Z.; Xu, D.; Du, C.; Li, X. Laboratory investigation of microbiologically influenced corrosion of Q235 carbon steel by halophilic archaea *Natronorubrum tibetense*. *Corros. Sci.* **2018**, *145*, 151–161. [CrossRef]
9. Enning, D.; Garrelfs, J. Corrosion of iron by sulfate-reducing bacteria: New views of an old problem. *Appl. Environ. Microbiol.* **2014**, *80*, 1226–1236. [CrossRef]
10. Kato, S. Microbial extracellular electron transfer and its relevance to iron corrosion. *Microb. Biotechnol.* **2016**, *9*, 141–148. [CrossRef]
11. Ma, Y.; Zhang, Y.; Zhang, R.; Guan, F.; Hou, B.; Duan, J. Microbiologically influenced corrosion of marine steels within the interaction between steel and biofilms: A brief view. *Appl. Microbiol. Biotechnol.* **2020**, *104*, 515–525. [CrossRef]
12. Tremblay, P.-L.; Angenent, L.T.; Zhang, T. Extracellular electron uptake: Among autotrophs and mediated by surfaces. *Trends Biotechnol.* **2017**, *35*, 360–371. [CrossRef] [PubMed]
13. He, S.; Barco, R.A.; Emerson, D.; Roden, E.E. Comparative genomic analysis of neutrophilic iron (II) oxidizer genomes for candidate genes in extracellular electron transfer. *Front. Microbiol.* **2017**, *8*, 1584. [CrossRef] [PubMed]
14. Shukla, S.K.; Khan, A.; Rao, T.S. Microbial fouling in water treatment plants. In *Microbial and Natural Macromolecules*; Elsevier: Amsterdam, The Netherlands, 2021; pp. 589–622.
15. Schmidt, T.M. *Encyclopedia of Microbiology*; Academic Press: Oxford, UK, 2019.
16. Beese-Vasbender, P.F.; Nayak, S.; Erbe, A.; Stratmann, M.; Mayrhofer, K.J. Electrochemical characterization of direct electron uptake in electrical microbially influenced corrosion of iron by the lithoautotrophic SRB *Desulfopila corrodens* strain IS4. *Electrochim. Acta* **2015**, *167*, 321–329. [CrossRef]
17. Chiu, B.K.; Kato, S.; McAllister, S.M.; Field, E.K.; Chan, C.S. Novel pelagic iron-oxidizing Zetaproteobacteria from the Chesapeake Bay oxic–anoxic transition zone. *Front. Microbiol.* **2017**, *8*, 1280. [CrossRef] [PubMed]
18. Baek, J.; Kim, C.; Song, Y.E.; Mutyala, S.; Seol, E.-H.; Kim, J.R. Bioelectrochemical metabolic regulation of a heterologously expressed glycerol reductive pathway in *E. coli* BL21 (DE3). *Electrochim. Acta* **2022**, *434*, 141260. [CrossRef]
19. Mutyala, S.; Kim, C.; Song, Y.E.; Khandelwal, H.; Baek, J.; Seol, E.; Oh, Y.-K.; Kim, J.R. Enabling anoxic acetate assimilation by electrode-driven respiration in the obligate aerobe, *Pseudomonas putida*. *Bioelectrochemistry* **2021**, *138*, 107690. [CrossRef]
20. Khandelwal, H.; Mutyala, S.; Kim, M.; Song, Y.E.; Li, S.; Jang, M.; Oh, S.-E.; Kim, J.R. Colorimetric isolation of a novel electrochemically active Pseudomonas strain using tungsten nanorods for bioelectrochemical applications. *Bioelectrochemistry* **2022**, *146*, 108136. [CrossRef]
21. Kim, M.; Li, S.; Kong, D.S.; Song, Y.E.; Park, S.-Y.; Kim, H.-I.; Jae, J.; Chung, I.; Kim, J.-R. Polydopamine/Polypyrrole Modified Graphite Felt Enhances Biocompatibility for Electroactive Bacteria and Power Density of Microbial Fuel Cell. *Chemosphere* **2023**, *313*, 137388. [CrossRef]
22. Huang, H.; Gong, C.S.; Tsao, G.T. Production of 1,3-propanediol by *Klebsiella pneumoniae*. In *Biotechnology for Fuels and Chemicals*; Springer: Totowa, NJ, USA, 2002; pp. 687–698.
23. Zhu, F.H.; Liu, D.H.; Chen, Z. Recent advances in biological production of 1,3-propanediol: New routes and engineering strategies. *Green Chem.* **2022**, *24*, 1390–1403. [CrossRef]
24. Kim, C.; Lee, J.H.; Baek, J.; Kong, D.S.; Na, J.G.; Lee, J.; Sundstrom, E.; Park, S.; Kim, J.R. Small Current but Highly Productive Synthesis of 1,3-Propanediol from Glycerol by an Electrode-Driven Metabolic Shift in *Klebsiella pneumoniae* L17. *ChemSusChem* **2020**, *13*, 564–573. [CrossRef]
25. Jensen, T.O.; Kvist, T.; Mikkelsen, M.J.; Westermann, P. Production of 1,3-PDO and butanol by a mutant strain of *Clostridium pasteurianum* with increased tolerance towards crude glycerol. *AMB Express* **2012**, *2*, 44. [CrossRef]
26. Mu, Y.; Teng, H.; Zhang, D.-J.; Wang, W.; Xiu, Z.-L. Microbial production of 1,3-propanediol by Klebsiella pneumoniae using crude glycerol from biodiesel preparations. *Biotechnol. Lett.* **2006**, *28*, 1755–1759. [CrossRef]
27. Asopa, R.P.; Ikram, M.M.; Saharan, V.K.J. Valorization of glycerol into 1,3-propanediol and organic acids using biocatalyst *Saccharomyces cerevisiae*. *Bioresour. Technol. Rep.* **2022**, *18*, 101084. [CrossRef]
28. Kong, D.S.; Kim, C.; Song, Y.E.; Baek, J.; Im, H.S.; Kim, J.R. Zero-valent iron driven bioconversion of glycerol to 1,3-propanediol using *Klebsiella pneumoniae* L17. *Process Biochem.* **2021**, *106*, 158–162. [CrossRef]

29. Zhou, S.; Lama, S.; Sankaranarayanan, M.; Park, S. Metabolic engineering of Pseudomonas denitrificans for the 1,3-propanediol production from glycerol. *Bioresour. Technol.* **2019**, *292*, 121933. [CrossRef]

30. Wong, N.; Jantama, K. Engineering Escherichia coli for a high yield of 1,3-propanediol near the theoretical maximum through chromosomal integration and gene deletion. *Appl. Microbiol. Biotechnol.* **2022**, *106*, 2937–2951. [CrossRef] [PubMed]

31. Kim, C.; Ainala, S.K.; Oh, Y.K.; Jeon, B.H.; Park, S.; Kim, J.R. Metabolic flux change in *Klebsiella pneumoniae* L17 by anaerobic respiration in microbial fuel cell. *Biotechnol. Bioproc. Eng.* **2016**, *21*, 250–260. [CrossRef]

32. Sakuntala, M.; Kim, J.R. Recent advances and challenges in the bioconversion of acetate to value-added chemicals. *Bioresour. Technol.* **2022**, *364*, 128064.

33. Kim, M.; Li, S.; Song, Y.E.; Lee, D.-Y.; Kim, J.R. Electrode-attached cell-driven biogas upgrading of anaerobic digestion effluent CO_2 to CH_4 using a microbial electrosynthesis cell. *Chem. Eng. J.* **2022**, *446*, 137079. [CrossRef]

34. Im, H.S.; Kim, C.; Song, Y.E.; Baek, J.; Im, C.H.; Kim, J.R. Isolation of novel CO converting microorganism using zero valent iron for a bioelectrochemical system (BES). *Biotechnol. Bioproc. Eng.* **2019**, *24*, 232–239. [CrossRef]

35. Kong, D.S.; Park, E.J.; Mutyala, S.; Kim, M.; Cho, Y.; Oh, S.E.; Kim, C.; Kim, J.R. Bioconversion of Crude Glycerol into 1,3-Propanediol (1,3-PDO) with Bioelectrochemical System and Zero-Valent Iron Using *Klebsiella pneumoniae* L17. *Energies* **2021**, *14*, 6806. [CrossRef]

36. Hidaka, T.; Tsuno, H.; Yagi, H.; Kosaka, Y. Fundamental analysis of real-time PCR quantification and modeling for thermophilic L-lactate fermentation by *Bacillus coagulans* from glucose. *Biotechnol. Bioproc. Eng.* **2012**, *17*, 290–297. [CrossRef]

37. Liu, J.L.; Ren, X.M.; Li, C.Z.; Wang, M.D.; Li, H.; Yang, Q.H. Assembly of COFs layer and electron mediator on silica for visible light driven photocatalytic NADH regeneration. *Appl. Catal. B-Environ.* **2022**, *310*, 121314. [CrossRef]

38. Lee, D.Y.; Yun, H.; Park, S.; Lee, S.Y. MetaFluxNet: The management of metabolic reaction information and quantitative metabolic flux analysis. *Bioinformatics* **2003**, *19*, 2144–2146. [CrossRef] [PubMed]

39. Kumar, V.; Park, S.J. Potential and limitations of *Klebsiella pneumoniae* as a microbial cell factory utilizing glycerol as the carbon source. *Biotechnol. Adv.* **2018**, *36*, 150–167. [CrossRef] [PubMed]

40. Jin, R.; Forage, R.; Lin, E. Glycerol kinase as a substitute for dihydroxyacetone kinase in a mutant of *Klebsiella pneumoniae*. *J. Bacteriol.* **1982**, *152*, 1303–1307. [CrossRef] [PubMed]

41. Jonsson, T.; Pujilaksono, B.; Hallstrom, S.; Agren, J.; Svensson, J.E.; Johansson, L.G.; Halvarsson, M. An ESEM in situ investigation of the influence of H_2O on iron oxidation at 500 degrees C. *Corros. Sci.* **2009**, *51*, 1914–1924. [CrossRef]

42. Bertrand, N.; Desgranges, C.; Poquillon, D.; Lafont, M.-C.; Monceau, D.J. Iron oxidation at low temperature (260–500 °C) in air and the effect of water vapor. *Oxid. Met.* **2010**, *73*, 139–162. [CrossRef]

43. Jonsson, T.; Pujilaksono, B.; Fuchs, A.; Svensson, J.E.; Johansson, L.G.; Halvarsson, M. The influence of H_2O on iron oxidation at 600 C: A microstructural study. *Mater. Sci. Forum* **2008**, *595*, 1005–1012. [CrossRef]

44. Ravi, S.; Karthikeyan, A.J. Magnetically tunable superparamagnetic cobalt doped iron oxide colloidal nanocluster. *Adv. Mater. Lett.* **2013**, *4*, 562–566. [CrossRef]

45. Deutzmann, J.S.; Sahin, M.; Spormann, A.M. Extracellular enzymes facilitate electron uptake in biocorrosion and bioelectrosynthesis. *mBio* **2015**, *6*, e00496-15. [CrossRef] [PubMed]

46. Li, Y.C.; Xu, D.K.; Chen, C.F.; Li, X.G.; Jia, R.; Zhang, D.W.; Sand, W.; Wang, F.H.; Gu, T.Y. Anaerobic microbiologically influenced corrosion mechanisms interpreted using bioenergetics and bioelectrochemistry: A review. *J. Mater. Sci. Technol.* **2018**, *34*, 1713–1718. [CrossRef]

47. Mori, K.; Tsurumaru, H.; Harayama, S. Iron corrosion activity of anaerobic hydrogen-consuming microorganisms isolated from oil facilities. *J. Biosci. Bioeng.* **2010**, *110*, 426–430. [CrossRef] [PubMed]

48. Lou, Y.T.; Chang, W.W.; Cui, T.Y.; Qian, H.C.; Huang, L.Y.; Ma, L.W.; Hao, X.P.; Zhang, D.W. Microbiologically influenced corrosion inhibition of carbon steel via biomineralization induced by *Shewanella putrefaciens*. *NPJ Mater. Degrad.* **2021**, *5*, 59. [CrossRef]